Effect of traveling magnetic field on solute distribution and dendritic growth in unidirectionally solidifying Sn–50 wt%Pb alloy: An in situ observation

Fei Cao [a], Fenfen Yang [a], Huijun Kang [a], Cunlei Zou [a], Tiqiao Xiao [b], Wanxia Huang [c], Tongmin Wang [a,*]

[a] Key Laboratory of Solidification Control and Digital Preparation Technology (Liaoning Province), School of Material Science and Engineering, Dalian University of Technology, Dalian 116024, China
[b] Shanghai Institute of Applied Physics, Chinese Academy of Sciences, Shanghai 201204, China
[c] Institute of High Energy Physics, Chinese Academy of Sciences, Beijing 100049, China

ABSTRACT

Synchrotron X-ray radiography was used to in situ study the solute distribution and the dendritic growth during the bottom-up solidification of Sn–50 wt%Pb alloy under a traveling magnetic field (TMF) for the first time. The buoyance driven evolution and motion of the plumes containing Sn-rich melt are directly observed in the solidification front before the application of TMF. A forced melt flow from left to right is induced with the application of TMF, which results in the redistribution of the solute concentration (facilitate the solute transportation and reduce the local fluctuations considerably) and the change of the dendrite morphologies (promote/suppress the growth of the secondary arms, remelting and fragmentation of dendrites). Meanwhile, the concentration variations of Sn around the solidification front are quantitatively analyzed through the extraction of gray level from sequenced X-ray images.

© 2016 Elsevier B.V. All rights reserved.

1. Introduction

The convection in a solidifying melt can significantly impact the solute distribution directly in metal alloys and hence the solidified microstructures which have an important influence on the mechanical properties of the materials [1,2]. Many studies have shown that the application of external fields on the solidifying melts is an effective method to achieve high quality castings, either directly by stirring [3,4] or indirectly by applying an electromagnetic field [5–7] or ultrasonic field [8,9]. Among all the above mentioned methods, electromagnetic field offers an efficient way for a contactless influence on the unsolidified melts, resulting in the convective transport of solute and the destabilization of growth conditions which lead to grain refinement and morphological change [10–14]. However, traditional experimental investigations are mainly restricted to a post-mortem analysis of the solidified microstructures [3,8,10–14] and fail to reveal the dynamic information about the interactive relationships between the

solute distribution and the microstructures formation under the electromagnetic field. Though experiments of transparent organic alloys [9,15–17] delivered valuable information for verification of solidification theories, these experiments do not really represent the situation in a solidifying metal alloys due to the differences in the thermophysical parameters. Now, synchrotron X-ray radiography with satisfying spatial and temporal resolution has become an important diagnostic tool for in situ and real time observation of solidification process in opaque metal alloys [18–23]. Only a few studies have been reported to study the effect of electromagnetically driven melt convection on the concentration profiles and the dendrite morphologies using X-ray radiography (synchrotron or laboratory source). Boden et al. [24] demonstrated how a specific flow pattern induced by electromagnetic stirring in Ga–25 wt%In alloy provokes a unidirectional solute transport in the mushy zone which in turn causes the formation of spacious segregation pattern. Liotti et al. [25] investigated the effect of a pulsed electromagnetic field on dendrite fragmentation in Al–15 wt%Cu alloy. The induced movement of interdendritic liquid between the primary and secondary dendrite arms was suggested to be the mechanism for the increased fragmentation rate. Shevchenko et al. [26] studied the effect of natural and

---

electromagnetically driven forced convection on dendritic solidification in Ga–25 wt%In alloy. The flow induced variation of the local solute concentration results in an unsteady development of the primary dendrites and promotes or inhibits the development of secondary and tertiary arms.

The present study is devoted to the visualization of the solute distribution and the dendritic growth during the bottom-up solidification of Sn–50 wt%Pb alloy using synchrotron X-ray radiography. The reasons to select the Sn–Pb alloy are as follows: (1) it have low solidus/liquidus temperatures making it easier for the designing of the furnace and the applying of the TMF; (2) the Sn–Pb phase diagram is well-known making it suited for exploratory work; (3) the large difference in X-ray absorption coefficient between Sn and Pb helps to produce good absorption contrast for getting clear images. In this work, we investigated the effect of melt flow on the redistribution of solute concentration and the dendrite morphologies with and without TMF.

2. Experimental

The experiments were carried out on the bending magnet beamline BL13W1 of Shanghai Synchrotron Radiation Facility (SSRF, China). Phase and absorption contrast synchrotron X-ray radiography was used to study the effect of TMF on solute distribution and dendritic growth in solidifying Sn–50 wt%Pb alloy. The synchrotron radiation experimental setup is schematically depicted in Fig. 1. The upper and lower plate heaters in Fig. 1 were aligned vertically in the vertical plane and separated by an adjustable gap through which X-rays passed through the sample cell. The sample cell was placed in close contact with both heaters. The TMF is generated by means of applying out-of-phase alternating-current (40 A) with the normal frequency of 50 Hz to the TMF generator which was placed at the bottom of the lower heaters. As a result, an electromagnetic force (EMF) from left to right is induced when a conductive melt (sample) was applied.

Sn–50 wt%Pb alloy samples were prepared by melting high purity Sn (99.99%) and Pb (99.99%) in an alumina crucible and cast into a cylindrical stainless steel mold. Cast ingots were then machined to the required sample dimensions (10×20 mm² in surface area and 500 μm in thickness) and thereafter ground and polished on both sides to 100 μm in thickness. Finally, the prepared foil sample was encapsulated between two ceramic plates. A hollow polytetrafluoroethylene (PTFE) sheet was also placed between the two ceramic plates to fix the sample.

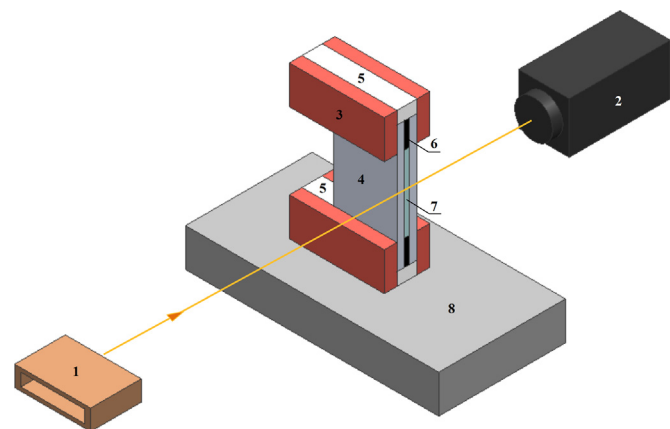The incident monochromatic X-ray with an energy of 26 keV

Fig. 1. Schematic of the synchrotron radiation experimental setup. 1: synchrotron radiation X-ray source; 2: CCD camera; 3: plate heater; 4: ceramic plate; 5: thermal insulation material; 6: mica sheet; 7: sample; 8: TMF generator.

was obtained through a Si double crystal monochromator, and then passed through the sample. A 200 μm thick YAG: Ce scintillator screen was used to convert the transmitted X-rays to visible light. The time-sequenced images were recorded by a PCO2000 charge coupled device (CCD) camera with 2048×2048 pixel array and a 14 bit dynamical range. The field of view at the selected magnification used for all experiments was 7.5×4.2 mm² with a satisfying spatial resolution (pixel size 3.7 μm $\times$ 3.7 μm). The exposure time per frame was 3 s and the distance from sample to detector was 40 cm.

A series of solidification experiments with and without TMF were carried out as follows. Firstly, both the upper and lower plate heaters were set to a temperature above the liquidus temperature of Sn–50 wt%Pb alloy. The lower heater temperature was reduced to trigger the solidification when the sample was completely melted and homogenously distributed. The temperature along the sample cell was measured by two embedded K-type thermocouples 1 cm away from each other. The cooling rate of the sample was $R=5$ K min^{-1}. The mean temperature gradient over the sample was $G=6.3$ K cm^{-1} for all experiments. As a consequence, the dendrite front grew from bottom to top (antiparallel g) unidirectionally. The TMF was applied after $t=247$ s when the dendrite front had occupied about one third of the field of view, $t=0$ s is assigned to the onset of cooling.

3. Results and discussion

Fig. 2 shows a sequence of images recorded during the solidification of Sn–50 wt%Pb alloy with and without TMF. Fig. 2(a)–(d) shows the solidification of Sn–50 wt%Pb alloy without TMF. The dark dendritic network denoted by the arrow corresponds to the primary Pb-rich dendrites growing from bottom to top. The Sn-rich zones can be identified in the interdendritic regions and in the vicinity of dendrite front as a result of solute rejection. The Sn-rich melt is less dense compared to the melt with initial composition. As a consequence, the melt density difference in different areas provokes the formation of ascending plumes containing Sn-rich melt. The variation of number, size and position of the plumes during the solidification are shown in Fig. 2(a)–(d). Many small plumes arise at the early stage of the solidification, and are well developed thereafter. The plumes span a distance of several millimeters and produce a long range diffusion of solute towards the melt region. Similar phenomena are also observed by Shevchenko et al. [26,27] in the solidification of Ga-In alloys. Moreover, the growth of dendrites are also affected by several small crystals ahead of the solidification front, see for instance the grains 1, 2 and 3 in Fig. 2. Finally, those small crystals are blocked by the overgrowing dendrite side arms. Fig. 2(e)–(h) shows the development of solute concentration field and the evolution of dendritic structure under the influence of TMF. A forced melt flow from left to right is induced when the TMF is applied. As a consequence, the well-developed upright ascending plumes becomes unstable and tends to incline to the right denoted by the red arrows in Fig. 2(e)–(g). Finally, the plumes on the right side of the solidification front gradually disappears. In the process of solidification, the growth of Pb-rich dendrites results in an accumulation of rejected Sn in the interdendritic zone. The solute pile-up alters the local compositional balance and lowers the melting point of the solid/liquid interface, causing the partly remelting of the dendritic structures labeled by the red ellipses in Fig. 2(h) [28,29]. As a consequence, small pieces of fragments detaches from the dendritic network and fall into the mushy zone. However, flow induced mechanical fragmentation is not observed directly in the present study.

The concentration variation of Sn can be reflected by the evolution of the gray level extracted from the sequenced radiographs.
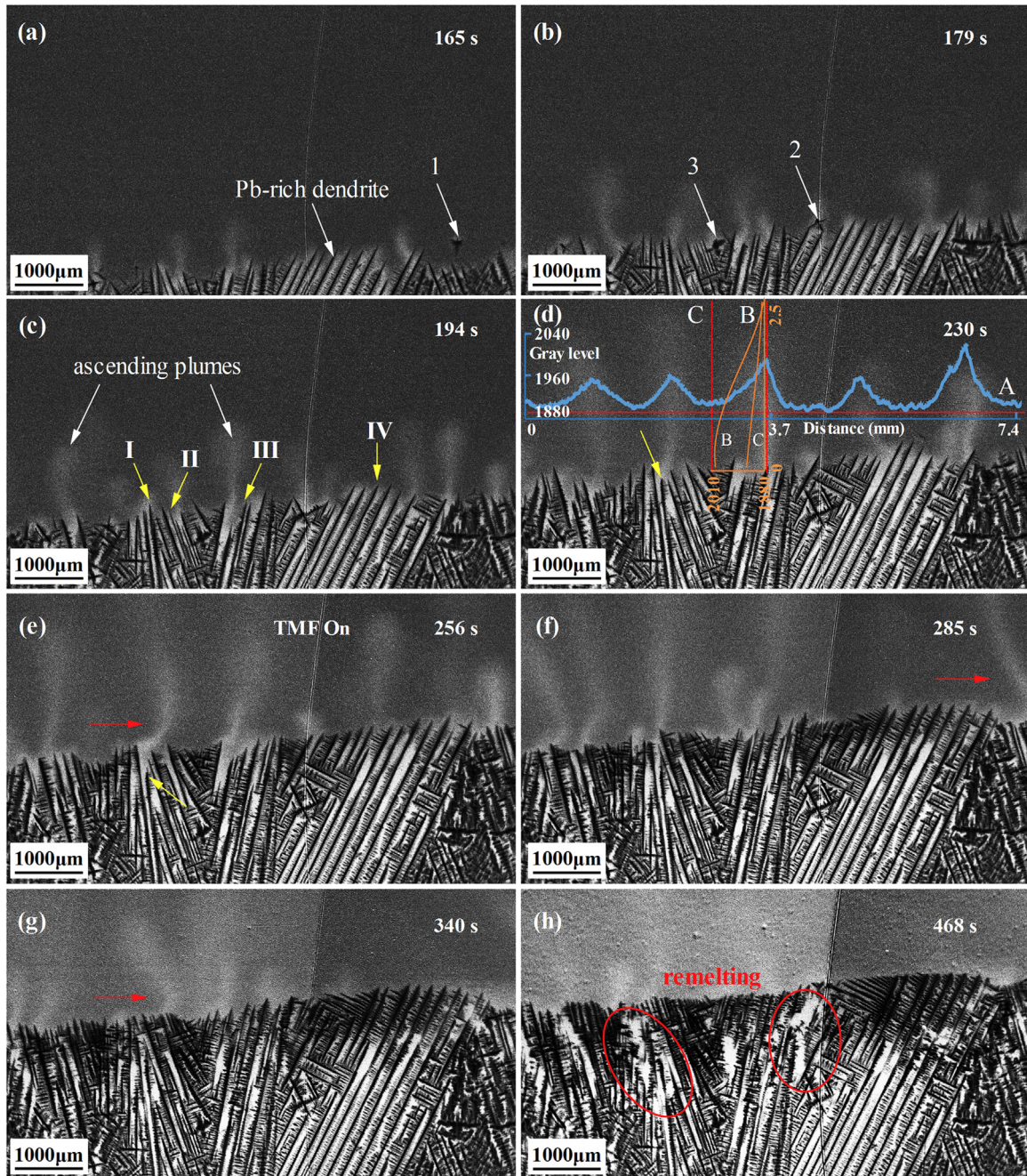
Fig. 2. Sequence of in situ radiographs showing the solute distribution and the dendritic growth during the solidification of Sn–50 wt%Pb alloy: (a)–(d) solidification without TMF; (e)–(f) solidification with TMF ($t=0$ s is assigned to the onset of cooling). The blue curve in Fig. 2(d) shows the gray level profile along the red horizontal line A. The orange curves in Fig. 2(d) show the gray level distribution along the vertical lines B and C, respectively. (For interpretation of the references to color in this figure legend, the reader is referred to the web version of this article.)

According to the equations $I=I_0 e^{-\mu_m m}$ and $\mu_m = K_4 \lambda^3 Z^3$, where I is the transmitted intensity, I_0 is the incident intensity, μ_m is the mass attenuation coefficient, m is the mass, K_4 is constant, λ is the wavelength of the X-ray and Z is the atomic number, the X-ray transmittance in Sn is higher than that in Pb as $Z_{Pb}(82) > Z_{Sn}(50)$. As a result, the higher the gray level, the higher Sn content in Sn–Pb system. The gray level curves are obtained by smoothing the measured points. The blue curve in Fig. 2(d) shows the gray level profile along the red horizontal line A. A wavy distribution of the Sn-rich melt along the solidification front is presented corresponding to the plume pattern. The orange curves in Fig. 2 (d) show the gray level distribution in the melt ahead of the solid–liquid interface measured at positions of vertical lines B and C, respectively. Higher solute concentration at the interface is found for the position of line B where plume occurs. It is indicated that the ascending plumes are accompanied by a downward flow of Sn-poor melt in the intermediate space, resulting in an in-homogeneous horizontal and vertical solute concentration distribution near the solidification front.

Fig. 3(a) displays the time evolution of the gray level at the solid–liquid interface in horizontal direction ($X=0$, starting from the left). A stable wavy distribution of the Sn-rich melt at the solidification front is disturbed when the TMF is applied. The significant fluctuation of the solute profile on the right side disappears gradually as a consequence of forced convection induced
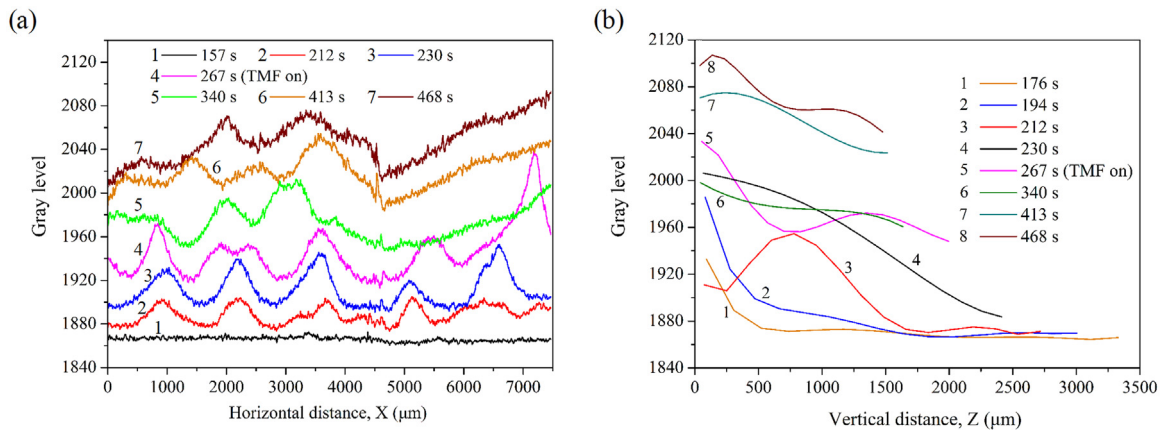
Fig. 3. Time evolution of the gray level ahead of the solid–liquid interface. (a) Gray value profile in horizontal direction at the interface; (b) gray value profile ahead of the interface front recorded along the vertical line B.

by the TMF. However, the fluctuation of the solute profile on the left side remains due to the existence of weak EMF in this area. Fig. 3(b) shows the gray value profile ahead of the interface ($Z=0$) front recorded along the vertical line B ($X=3622.3$ μm) at different time. It is obvious that the solute concentration undergoes strong variations. Besides, the concentration gradient with TMF is smaller than that without TMF, which indicates that the solute transport ahead of the solidification front is facilitated by the TMF. The apparent variations in the solute profile could affect the growth rate of the dendrite tip, which will be discussed later.

Fig. 4 shows the growth rates of the four selected dendrites (I, II, III and IV) with different inclination angles marked in Fig. 2(c). The growth rates of the dendrites are derived from the measurements of the solidified length between two successive X-ray radiographs. The remarkable fluctuation of the growth rates appears as a prominent feature of the solidification process without TMF. Video 1 (see Supplementary material) demonstrates that the fluctuations are strongly correlated with the variation of solute concentration at the solidification front. The solute distribution ahead of the solidification front results in the depression of the dendrite tip growth at the plume positions (peak value in Fig. 3 (a)). Thus the dendrite tip positions fall behind the neighboring regions where no plume exists. As a result, the growth rates of the adjacent dendrite are alternatively changed corresponding to the plumes patterns. Besides, the growth of the dendrite I stops earlier than the other dendrites as a result of the blocking of the adjacent
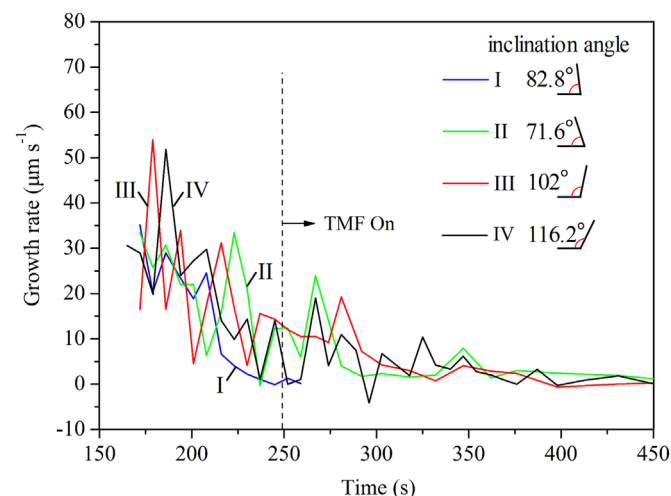
dendrites. This kind of competitive growth between the dendrite I and the adjacent dendrite can be observed in Fig. 2(d)–(e). The growth velocity rises with the application of TMF. The TMF induced forced melt flow ahead of the solidification front facilitates the Sn-rich melt transportation and reduces the local fluctuations of Sn solute concentration at the dendrites tips, which results in the increase of undercooling. No significant differences between the dendrite tip velocities of the four dendrites with different inclination angles are found under the TMF.

Supplementary material related to this article can be found online at http://dx.doi.org/10.1016/j.jcrysgro.2016.06.034.

When the TMF is applied, the secondary arms of dendrites with different inclination angles exhibit different growth behaviors, as shown in Fig. 2(e)–(h) (or see Supplementary material video 1). The preferential growth of the secondary arms is observed at the down flow sides of the primary dendrite arms with an inclination angle of 71.6° (dendrite II). Whereas the preferential growth is observed at the incoming flow sides of the primary dendrite arms with an inclination angle of 116.2° (dendrite IV). On the contrary, the growth of the secondary arms at the opposite sides of the primary dendrite arms (dendrite II and IV) is suppressed. Besides, no obvious preferential growth of the secondary arms is observed on both sides of the primary dendrite arms with an inclination angle of 102° (dendrite III). Fig. 5 shows the schematic of the interaction between the forced melt flow and the dendrites with different inclination angles to illustrate the mechanism of the growth behavior of the secondary arms under TMF. As shown in
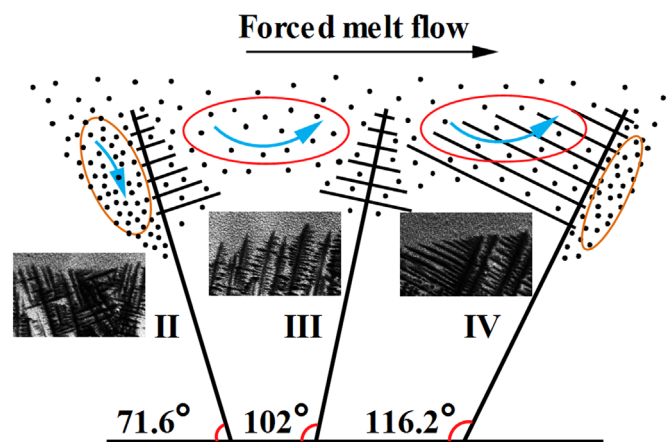

Fig. 4. The time evolution of the dendrite tip velocity of the four dendrites with different inclination angles marked in Fig. 2(c).

Fig. 5. Schematic of the interaction between the forced melt flow and the dendrites with different inclination angles. (For interpretation of the references to color in this figure legend, the reader is referred to the web version of this article.)

Fig. 5, the Sn-rich melt at the left side of dendrite II and the right side of dendrite IV (orange elliptic areas in Fig. 5) is not easy to be transported into the melt with melt flow from left to right. As a consequence, the growth of the secondary arms in these areas is suppressed due to the solute enrichment. While the Sn-rich melt transportation at the red elliptic areas shown in Fig. 5 is enhanced by the forced melt flow, which facilitates the growth of secondary arms. The growth behavior of the secondary arms on both sides of dendrite III (approximately normal) is similar since the Sn-rich melt on both sides of the primary dendrite III can be easily washed away. In a word, the orientation of the forced melt flow with respect to the growth directions of the primary dendrites (i.e. inclination angle) have an influence on the growth of the secondary arms on both sides of the primary dendrite arms.

4. Conclusions

The solute distribution and the dendritic growth during the bottom-up solidification of Sn–50 wt%Pb alloy under TMF were investigated by synchrotron X-ray radiography. The buoyance driven evolution and motion of the plumes containing Sn-rich solute are directly observed before the application of TMF. The advancement of the solidification front at the plume positions is suppressed and the dendrite tip positions fall behind the neighboring regions where no plume exists. A forced melt flow from left to right is induced with the application of TMF. The forced melt flow ahead of the solidification front facilitates the solute transportation and reduces the local fluctuations of solute concentration considerably. Preferential growth of the secondary arms is observed at the incoming flow and down flow sides of the primary dendrite arms with obtuse angle and acute angle, respectively. Whereas the growth of the secondary arms at the opposite sides of the primary dendrite arms is suppressed due to the high Sn solute concentration. The growth of the secondary arms on both sides of primary dendrite arms with approximately right angle is also facilitated since the Sn-rich melt on both sides can be easily washed away. Besides, remelting and fragmentation of dendrites due to the solute enrichment are also observed. But the flow induced mechanical fragmentation is not found in the direct observation.

References

[1] R. Trivedi, P. Mazumder, S.N. Tewari, The effect of convection on disorder in primary cellular and dendritic arrays, Metall. Mater. Trans. A 33 (2002) 3763–3775.
[2] H. Nguyen Thi, Y. Dabo, B. Drevet, M.D. Dupouy, D. Camel, B. Billia, J.D. Hunt, A. Chilton, Directional solidification of Al-1.5 wt% Ni alloys under diffusion transport in space and fluid-flow localisation on earth, J. Cryst. Growth 281 (2005) 654–668.
[3] D. Brabazon, D.J. Browne, A.J. Carr, Mechanical stir casting of aluminium alloys from the mushy state: process, microstructure and mechanical properties, Mater. Sci. Eng. A 326 (2002) 370–381.
[4] Z. Fan, Semisolid metal processing, Int. Mater. Rev. 47 (2002) 49–85.
[5] S. Asai, Recent development and prospect of electromagnetic processing of materials, Sci. Technol. Adv. Mater. 1 (2000) 191–200.
[6] H.K. Moffatt, Electromagnetic stirring, Phys. Fluids A 3 (1991) 1336–1343.
[7] P. Davidson, Magnetohydrodynamics in materials processing, Annu. Rev. Fluid. Mech. 31 (1999) 273–300.
[8] R. Haghayeghi, P. Kapranos, Solidification of Pb-Sn alloys under ultrasonic field, Mater. Lett. 126 (2014) 244–248.
[9] D. Shu, B. Sun, J. Mi, P. Grant, A high-speed imaging and modeling study of dendrite fragmentation caused by ultrasonic cavitation, Metall. Mater. Trans. A 43 (2012) 3755–3766.
[10] L. Wang, J. Shen, L. Qin, Z. Feng, L. Wang, H. Fu, The effect of the flow driven by a travelling magnetic field on solidification structure of Sn–Cd peritectic alloys, J. Cryst. Growth 356 (2012) 26–32.
[11] Y.J. Li, W.Z. Tao, Y.S. Yang, Grain refinement of Al–Cu alloy in low voltage pulsed magnetic field, J. Mater. Process. Technol. 212 (2012) 903–909.
[12] J.C. Jie, Q.C. Zou, J.L. Sun, Y.P. Lu, T.M. Wang, T.J. Li, Separation mechanism of the primary Si phase from the hypereutectic Al–Si alloy using a rotating magnetic field during solidification, Acta Mater. 72 (2014) 57–66.
[13] L. Hachani, K. Zaidat, Y. Fautrelle, Experimental study of the solidification of Sn–10 wt%Pb alloy under different forced convection in benchmark experiment, Int. J. Heat Mass Transf. 85 (2015) 438–454.
[14] E.J. Zoqui, M. Paes, E. Es-Sadiqi, Macro- and microstructure analysis of SSM A356 produced by electromagnetic stirring, J. Mater. Process. Technol. 120 (2002) 365–373.
[15] E. Çadırlı, İ. Karaca, H. Kaya, N. Maraşli, Effect of growth rate and composition on the primary spacing, the dendrite tip radius and mushy zone depth in the directionally solidified succinonitrile–Salol alloys, J. Cryst. Growth 255 (2003) 190–203.
[16] J. Teng, S. Liu, R. Trivedi, Onset of sidewise instability and cell-dendrite transition in directional solidification, Acta Mater. 57 (2009) 3497–3508.
[17] S.S.L. Peppin, H.E. Huppert, M.G. Worster, Steady-state solidification of aqueous ammonium chloride, J. Fluid. Mech. 599 (2008) 465–476.
[18] R. Mathiesen, L. Arnberg, F. Mo, T. Weitkamp, A. Snigirev, Time resolved x-ray imaging of dendritic growth in binary alloys, Phys. Rev. Lett. 83 (1999) 5062.
[19] G. Reinhart, C.A. Gandin, N. Mangelinck-Noël, H. Nguyen-Thi, J.E. Spinelli, J. Baruchel, B. Billia, Influence of natural convection during upward directional solidification: a comparison between in situ X-ray radiography and direct simulation of the grain structure, Acta Mater. 61 (2013) 4765–4777.
[20] T.M. Wang, F. Cao, P. Zhou, H.J. Kang, Z.N. Chen, Y.N. Fu, T.Q. Xiao, W.X. Huang, Q.X. Yuan, Study on diffusion behavior and microstructural evolution of Al/Cu bimetal interface by synchrotron X-ray radiography, J. Alloy. Compd. 616 (2014) 550–555.
[21] H. Yasuda, I. Ohnaka, K. Kawasaki, A. Sugiyama, T. Ohmichi, J. Iwane, K. Umetani, Direct observation of stray crystal formation in unidirectional solidification of Sn–Bi alloy by X-ray imaging, J. Cryst. Growth 262 (2004) 645–652.
[22] G. Reinhart, A. Buffet, H. Nguyen-Thi, B. Billia, H. Jung, N. Mangelinck-Noel, N. Bergeon, T. Schenk, J. Hartwig, J. Baruchel, In-Situ and real-time analysis of the formation of strains and microstructure defects during solidification of Al-3.5 wt pct Ni alloys, Metall. Mater. Trans. A 39A (2008) 865–874.
[23] T.M. Wang, F. Cao, Z.N. Chen, H.J. Kang, J. Zhu, Y.N. Fu, T.Q. Xiao, T.J. Li, Three dimensional microstructures and wear resistance of Al–Bi immiscible alloys with different grain refiners, Sci. China Technol. Sci. 58 (2015) 870–875.
[24] S. Boden, S. Eckert, G. Gerbeth, Visualization of freckle formation induced by forced melt convection in solidifying GaIn alloys, Mater. Lett. 64 (2010) 1340–1343.
[25] E. Liotti, A. Lui, R. Vincent, S. Kumar, Z. Guo, T. Connolley, I.P. Dolbnya, M. Hart, L. Arnberg, R.H. Mathiesen, P.S. Grant, A synchrotron X-ray radiography study of dendrite fragmentation induced by a pulsed electromagnetic field in an Al–15Cu alloy, Acta Mater. 70 (2014) 228–239.
[26] N. Shevchenko, O. Roshchupkina, O. Sokolova, S. Eckert, The effect of natural and forced melt convection on dendritic solidification in Ga–In alloys, J. Cryst. Growth 417 (2015) 1–8.
[27] N. Shevchenko, S. Boden, G. Gerbeth, S. Eckert, Chimney formation in solidifying Ga-25wt pct In alloys under the influence of thermosolutal melt convection, Metall. Mater. Trans. A 44A (2013) 3797–3808.
[28] M. Rettenmayr, Melting and remelting phenomena, Int. Mater. Rev. 54 (2009) 1–17.
[29] D. Ruvalcaba, R.H. Mathiesen, D.G. Eskin, L. Arnberg, L. Katgerman, In situ observations of dendritic fragmentation due to local solute-enrichment during directional solidification of an aluminum alloy, Acta Mater. 55 (2007) 4287–4292.